Electrostatic properties of inner nanopore surfaces of anodic aluminum oxide membranes upon high temperature annealing revealed by EPR of *p*H-sensitive spin probes and labels

Elena G. Kovaleva [a,**], Leonid S. Molochnikov [b], Daria Tambasova [a], Antonin Marek [c], Melanie Chestnut [c], Victoria A. Osipova [d], Denis O. Antonov [a], Igor A. Kirilyuk [e], Alex I. Smirnov [c,*]

[a] *Ural Federal University Named After the First President of Russia B N Yeltsin, Institute of Chemical Engineering, Mira St., 19, 620002, Yekaterinburg, Russian Federation*
[b] *Department of Chemistry, Ural State Forest Engineering University, Siberian Highway, 37, 620100, Yekaterinburg, Russian Federation*
[c] *Department of Chemistry, North Carolina State University, 2620 Yarbrough Drive, Raleigh, NC, 27695-8204, USA*
[d] *Laboratory of Organic Materials, I. Ya. Postovsky Institute of Organic Synthesis, Ural Branch of the Russian Academy of Sciences, 620990, Ekaterinburg, Akademicheskaya / S. Kovalevskoi, 22/20, Russian Federation*
[e] *Institute of Organic Chemistry, Siberian Branch of the Russian Academy of Sciences, Akad. Lavrent'ev Av. 9, 630090, Novosibirsk, Russian Federation*

ARTICLE INFO

ABSTRACT

Anodic aluminum oxide (AAO) membranes are versatile nanomaterials that combine the chemically stable and mechanically robust properties of ceramics with homogeneous nanoscale organization that can be tuned to desirable pore diameters and lengths. The AAO substrates feature high surface area that is readily accessible to large and small molecules, making these nanostructures uniquely suited for many possible applications. Examples include templated self-assembly of macroscopically aligned biological membranes and substrates for heterogeneous catalysis. For further development of such applications, one would like to characterize and tune the electrostatic properties of the inner pore surface as well as the local acidity within the nanochannels. Here, we employed electron paramagnetic resonance (EPR) spectroscopy of a small molecule – ionizable nitroxide – as a reporter of the average local acidity in the nanochannels and the local electrostatic potential in the immediate vicinity of the pore surface. The former was achieved by measuring EPR spectra of this molecular probe diffusing in an aqueous phase confined in the AAO nanochannels while for the latter the nitroxide was covalently attached to the hydroxyl group of the alumina surface. We show that the local acidity within the nanochannels is increased by as much as ≈1.48 *p*H units *vs.* the *p*H of bulk solution by decreasing the pore diameter down to *ca.* 31 nm. Furthermore, the positive surface charge of the as-prepared AAO could be decreased and even switched to a negative surface charge upon annealing the membranes first to 700 °C and then to 1200 °C. For as-prepared AAO, the local electrostatic potential reaches ψ= (163 ± 5) mV for the nitroxide label covalently attached to AAO and located about 0.5 nm away from the surface. Overall, we demonstrate that the acid-based properties of the aqueous volume confined by the AAO nanopores pores can be tuned by either changing the pore diameter from *ca.* 71 to 31 nm or by thermal annealing to switch the sign of the surface charge. These observations provide a simple and robust means to tailor these versatile high-surface-area nanomaterials for specific applications that depend on acid-base equilibria.

1. Introduction

Ceramic nanoporous membranes based on anodic aluminum oxide (AAO) are of a special interest for nano- and biotechnology for the reasons of a favorable combination of physical and chemical properties and the facile and inexpensive electrochemical fabrication methods. The

* Corresponding author.
** Corresponding author.
   E-mail addresses: gek1969@bk.ru (E.G. Kovaleva), Alex_Smirnov@ncsu.edu (A.I. Smirnov).

pore formation in AAO relies on a self-assembly rather than lithography or templating although the quality of the membranes could be further improved by the latter methods [1,2]. When fabricated following the two-step anodization procedure originally described by Masuda and Fukuda [3], the pores in the AAO films are macroscopically homogeneous and hexagonally packed with the pore diameter tunable over an exceptionally broad range of *ca.* 10–400 nm and density of *ca.* 10^8-10^{10} pores/cm^2 [1,2]. The inner surface of the AAO pores is easily accessible to chemicals and can be readily modified by a number of chemical and physical methods including silanization at room temperature [4–7], sol−gel deposition [8–10], electrochemical and electroless depositions (ECD and ELD) [11–15], chemical vapor deposition (CVD) [16,17], and atomic layer deposition (ALD) [18,19] among the others. Given the versatility of the surface modifications, the use of AAO membranes in such important fields as energy generation and storage [20], electronics and photonics [21–24], sensors and biosensors [25], drug delivery matrices [26], as well as in a form of versatile nanofabrication templates [2] has been rapidly accelerating in the recent years.

In terms of bio-/nano-applications, the AAO membranes have been shown to be suitable for encapsulating lipid bilayers and membrane proteins embedded in lipids while keeping these self-assembled structures fully hydrated and solvent-accessible [27–33]. An essential feature of the lipid bilayer membranes confined in AAO is a high degree of macroscopic alignment that enables structure determination of integral membrane proteins by oriented sample solid-state NMR (*e.g.* Refs. [28, 32,34]). This use of AAO membranes as nanotemplates for macroscopic alignment of molecules was further explored by Chen et al. who have achieved a controlled orientation of spin-correlated radical pairs by covalently linking such molecules to the AAO pore surface [35]. Such ordered multi-spin assemblies are viewed as essential prerequisite for developing solid-state molecule-based spintronics [*ibid.*]. AAO could also serve as a high surface area substrate for catalytically active organic and bio-organic groups and enzymes and also as an adsorbent for molecular separation [1,2]. The latter sorption and catalytic processes are known to be *p*H-dependent [36–42] but the local *p*H in the channels with nanoscale diameters does not necessarily follow acidity of the surrounding bulk aqueous phase [43]. For such systems, measurements of local acidity and electrostatic potential of the inner pore surfaces represent a problem of a great practical interest.

Recently, we reported on acid-base and electrostatic properties of pristine commercial AAO membranes and those prepared in-house from low-cost commercial grade aluminum [44]. We have also studied hydrated mesoporous and nanostructured γ-, basic γ-, α-alumina powders both in the pristine forms and modified with negatively charged phospholipids, aluminum butoxides and glycerates [45]. Both studies were carried out by EPR spectroscopy of *p*H-sensitive spin probes, which contain basic nitrogen functionalities in the heterocyclic ring [46]. The protonation of such functionality changes intermolecular electric field that affects the nitroxide magnetic parameters, such as nitrogen hyperfine coupling **A**-tensor and **g**-factor matrix [47]. Furthermore, the ns-scale rotational dynamics of charges and uncharged nitroxides in the proximity of charged surfaces could be strikingly different as reflected by the nitroxide continuous wave (CW) EPR spectra [48,49]. These phenomena make EPR spectra of such nitroxides exceptionally sensitive to local *p*H [50,51]. Because the method is based on EPR detection, it is fully applicable to opaque and not transparent samples such as nano- and mesoporous materials we studied.

The preceding EPR studies have shown that internal *p*H$_{int}$ in the pores of AAO membranes with diameters greater than or equal to 58 nm would essentially follow *p*H$_{ext}$ of the bulk external solution from 0.1 to 3.0 M range of the ionic strength, whereas the apparent *p*K$_a$ of nitroxide probes inside the nanopores of smaller diameters of 29 and 18 nm were found to be lower by 0.5–0.8 of *p*H units *vs.* bulk *p*H$_{ext}$ values [44]. The direction of the observed *p*K$_a$ shift was indicative of the pore surfaces having a positive charge. The sign of the charge is consistent with the surface layer composed of amorphous aluminum when the AAO

membranes are formed by anodization at low ($\leq$100 V) voltages [52, 53]. Depending on the anodization conditions, such an amorphous layer is known to contain varying amount of water [54] as well as some minor impurities attributed to the anions incorporated from the electrolyte [55]. Coordination environment of the aluminum atoms in the amorphous layer has been considered to be closely related to γ-Al$_2$O$_3$ with tetra- and hexa-coordinated aluminum cations in about 1:2 ratio [2]. While the surface hydroxyl (−OH) groups are abundant and suitable for chemical modifications [1], this amorphous layer is highly labile to both the acid and the base attacks.

Chemical stability of AAO can be greatly improved by a consequent heat treatment resulting in a gradual loss of water molecules and a series of polymorphic transformations such as crystallization into an almost pure γ-Al$_2$O$_3$ phase at 820–900 °C and then formation of metastable δ- and θ-Al$_2$O$_3$ phases which would further convert into thermodynamically stable α-Al$_2$O$_3$ above *ca.* 1150 °C [2,53,56]. One would expect all these phase transformations to affect the acid-base and surface electrostatic properties, which, in turn, determine catalytic and sorbent properties of these versatile nanoporous membranes. Some of these properties may also be dependent on the nanoscale pore diameter and the thickness of the initial amorphous alumina layer that could be etched away during the pore enlargement process. Thus, the main objective of this work was to study the relationships between the acid-base properties, surface charge, and the pore surface electrostatic potential, Ψ, of AAO membranes with average pore diameters ranging from *ca.* 31 to 71 nm and the effects of the annealing conditions on those. Compared to our preceding studies [44], the morphology of the AAO membranes was greatly improved by using high grade aluminum foil (99.997% pure) as the starting material and by implementing the two-step anodization procedure [3]. A different *p*H-sensitive nitroxide radical (NR, 4-dimethylamino-5,5-dimethyl-2-(4-(chloromethyl) phenyl)-2-ethyl-2,5-dihydro-1*H*-imidazol-1-oxyl hydrochloride semi-hydrate) was employed as either a spin probe (*i.e.*, when dissolved in an aqueous phase) or a spin label (*i.e.*, when covalently attached to the pore surface) to report on local *p*H and acid-base pore surface properties from changes in the experimental continuous wave (CW) X-band (9 GHz) EPR spectra.

2. Experimental Section

2.1. General

All chemicals of the ACS Reagent grade or higher were purchased from Sigma Aldrich/Merck, KGaA (Darmstadt, Germany) or VWR International, LLC (Radnor, PA, USA) unless otherwise indicated.

IR spectra were recorded using Bruker (Bruker Optik GmbH., Ettlingen, Germany) Vector 22 FT-IR spectrometer in neat samples.

To confirm structure of nitroxide 4-dimethylamino-2-(4-(dimethylaminomethyl)phenyl)-2-ethyl-5,5-dimethyl-2,5-dihydro-1*H*-imidazole-1-oxyl (NRD) 5% solution of the nitroxide (0.5 ml, 0.08 mmol) in CD$_3$OD was prepared and N$_2$D$_4$ (0.05 ml, 1.4 mmol) was added. The solution was kept at ambient temperature in an NMR tube until yellow color disappeared due to nitroxide reduction to the corresponding hydroxylamine over a period of *ca.* 48 h. The NMR ^{1}H spectrum was acquired at 300 K using Bruker (Bruker BioSpin GmbH, Silberstreifen, Germany) AM 400 spectrometer operating at 400.134 MHz ^{1}H Larmor frequency).

High-resolution mass spectra (HRMS, electron impact, 70 eV, temperature of vaporizer 270–300 °C) were recorded using a DFS Thermo Scientific mass spectrometer (Thermo Fisher Scientific, Waltham, MA USA).

2.2. Anodic aluminum oxide membranes

AAO membranes (AAO-1, AAO-2, AAO-4) with average pore diameters 31, 37, and 71 nm, respectively, and the pore length of *ca.* 50 μm were fabricated at NCSU following a two-step anodization process

similar to the one described by Masuda and Fukuda [3]. A high purity aluminum foil (99.997%, 0.127 mm thick, Strem Chemicals, Inc., Newburyport, MA, USA) was chosen as the starting material. The foil was cut into 76 mm × 102 mm sheets which were heat treated at 500 °C for 3 h to release stress. Consequently, the foil was electro-chemically polished at 20 V in 95:5 (v/v) mixture of 85 wt% H_3PO_4 and 97 wt% H_2SO_4 containing 20 g/l CrO_3 and then thoroughly cleaned in deionized water. Only the front side of the foil was subjected to the anodization while the back side was masked by a clear nail polish (Electron Microscopy Sciences, Hatfield, PA, USA). Anodization was carried out at 40 V in 4 wt% $H_2C_2O_4$ for 25 h for both steps. AAO from the first step was removed by exposing the anodized sample to an aqueous solution of 3.5 vol% H_3PO_4 and 45 g/l CrO_3 at 90 °C for 5–10 min and the second anodization step was started immediately thereafter. After completing the second anodization step the protective layer formed by the nail polish was removed by rinsing the sample with acetone. A thin back side aluminum oxide layer was removed by floating pieces on a surface of 10 vol% of aqueous solution of H_3PO_4 for about 2 h. Remaining metallic aluminum was dissolved in 10 wt% aqueous $CuCl_2$ solution at room temperature under a mild ultrasonic sonication. In order to open the nanopores from the terminating end the sample was treated with 10 wt% H_3PO_4 aqueous solution until a perspiration through the pores became visible. The pore diameter was further fine-tuned by etching the membranes in 5 wt% H_3PO_4 aqueous solution for a controlled time. At the end of the procedure, the samples were thoroughly rinsed in deionized water and air-dried.

Fabrication procedures for AAO-3 (39 nm average pore diameter) were the same as above except a thicker aluminum sheet (0.20 mm) was used as the starting material and the second anodization step was extended from *ca.* 24 to 85 h. These fabrication conditions resulted in a thicker ≈170 μm AAO with more robust mechanical properties allowing for further thermal analysis and sample annealing.

Measurements of mass changes and thermal effects for AAO-3 upon heating were carried out simultaneously using NETZSCH STA 449 F3 Jupiter® thermal analyzer (NETZSCH-Gerätebau GmbH., Selb, Germany) by placing the sample into a corundum crucible. A sharp peak at *ca.* 899.3 °C was detected by DSC and was accompanied by an immediate drop of mass by *ca.* −4.71 wt% (see Fig. S1 of the Supplemental Information). The DSC peak was attributed to a formation of the γ-alumina phase [53,57]. The AAO-3 samples were held at the annealing temperatures, 900 °C or 1200 °C, for 1 h. The heating and cooling rates of 20 and 1 °C/min, respectively, were chosen to prevent a thermal cracking and curling of the AAO membranes reported previously by other authors [58]. The same annealing conditions were then applied to treat larger batches of AAO-3 in a Thermo Scientific (Waltham, MA, USA) tube furnace while maintaining a constant air flow of 50 ml/min. For all EPR experiments the AAO sheets were laser-cut into 3 mm × 8 mm pieces to fit into standard EPR tubes.

The pore morphology and averaged diameters of all the fabricated AAO before the annealing were examined by either JEOL 2000FX (JEOL USA, Inc., Peabody, MA, USA) or Verios 460L (FEI, Inc., Hillsboro, OR, USA) SEM instruments installed at and operated by the NCSU Analytical Instrumentation Facility (AIF). For SEM imaging small pieces of AAO (about 3 mm × 3 mm) were cut from larger membranes and mounted on a sample holder using a double-sided carbon tape (Electron Microscopy Sciences). To suppress sample charging artifacts low accelerating potentials (*e.g.*, ≈1 kV for FEI Verios 460L) were employed. The pore diameters were analyzed directly from the SEM images using in-house script developed from an image processing toolbox of Matlab (Mathworks, Inc., Natick, MA, USA).

2.3. pH-sensitive nitroxides and covalent attachment of spin-label to AAO nanopore surfaces

*p*H-sensitive nitroxide radical (NR, 4-dimethylamino-5,5-dimethyl-2-(4-(chloromethyl) phenyl)-2-ethyl-2,5-dihydro-1*H*-imidazol-1-oxyl

hydrochloride semi-hydrate, Table 1) employed in this work as either a spin probe (when dissolved in water) or a spin label (when reacted with aminopropylethoxysilane and then covalently attached to the surface hydroxyl groups) was synthesized at the Institute of Organic Chemistry, Siberian Branch of the Russian Academy of Sciences (Novosibirsk, Russia) using the procedures described earlier [45]. This spin probe has $pK_a = 5.82 \pm 0.05$ at room temperature when dissolved in water (Table 1), thus, demonstrating *p*H-sensitivity over the range of *ca.* 4.9–6.9 *p*H units [45].
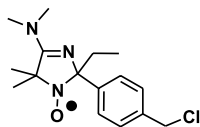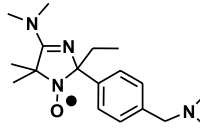
NR-dimethylamine (NRD, Table 1) adduct was prepared via treatment of NR with liquid cold dimethylamine. The mixture of NR hydrochloride semi-hydrate (177 mg, 0.5 mmol), $NaHCO_3$ (170 mg, 2 mmol), diethyl ether (15 ml) and water (15 ml) was vigorously shaken until the nitroxide NR was completely dissolved. The organic phase was separated, dried over Na_2SO_4 and the solvent was evaporated under reduced pressure. The residue was cooled to 0 °C and dissolved in liquid cold dimethylamine (3 ml, 46 mmol). The solution was allowed to stand at 0 °C for 1 h, the solvent was then allowed to evaporate at room temperature, and the residue was separated using column chromatography on basic alumina, eluent diethyl ether - hexane 1:1 to give NRD as a yellow oil, yield 140 mg (88%). Found, %: C, 68.41; H, 8.95; N, 17.33. Calculated for $C_{18}H_{29}N_4O$: C, 68.10; H, 9.21; N, 17.65. ν_{max} (KBr)/cm^{-1} 2973, 2937, 2875, 2858, 2813, 2765 (C–H), 1602 (C=N). HRMS (EI/DFS) *m/z* $[M+1]^+$ calcd for $(C_{18}H_{30}N_4O)^+$: 318.2410; found: 318.2414; $[M]^+$ calcd for $(C_{18}H_{30}N_4O)^+$: 317.2336; found: 317.2345. ^{1}H NMR (400 MHz; $CD_3OD + N_2D_4$, δ): 0.86 (br t, 3H), 0.93 (s, 3H), 1.44 (s, 3H), 1.99 (br m, 2H), 2.24 (s, 6H); 3.10 (s, 6H), 3.48 (s, 2H), 7.27 (br m, 2H) 7.52 (br m, 2H). See Figs. S2 and S3 of the Supplemental Information for experimental ^{1}H NMR and IR spectra.

For surface modification of AAO-2 membranes, NR (5 mg) was co-dissolved in 5 ml of acetonitrile together with 3.4 μl of aminopropylethoxysilane (APTES) and 4 μl of trimethylamine and left for 12 h at room temperature under a constant stirring. Consequently, 5 strips of the pristine AAO-2 membranes (53.5 mg total weight) were immersed into the solution and kept for another 12 h at room temperature under a constant stirring (Scheme 1). Next, the supernatant fluid was decanted, the AAO strips were washed with acetonitrile, and then followed by a further decantation and drying under argon.

2.4. EPR and potentiometric titration experiments

For EPR titrations the ratio between AAO and aqueous NR solution

Table 1
Molecular structure, pK_a, and isotropic nitrogen hyperfine coupling constants, *a*, of *p*H-sensitive nitroxide radicals employed in this study.[a]

Radical	Structural formula	pK_a, ±0.05[b]	a, ± 0.05, G[c]	
			RH$^+$	R
NR		5.82	14.60	15.44
NRD		5.76	14.54	15.44

[a] *g*-factors of the protonated and deprotonated forms of nitroxides in aqueous solution are not given because of negligible (in the fourth decimal digit) differences in their values.
[b] Standard errors were derived from least squares fitting of EPR titration curves.
[c] Standard errors were derived from least squares fitting of experimental EPR spectra using the standard covariance matrix method [59,60].
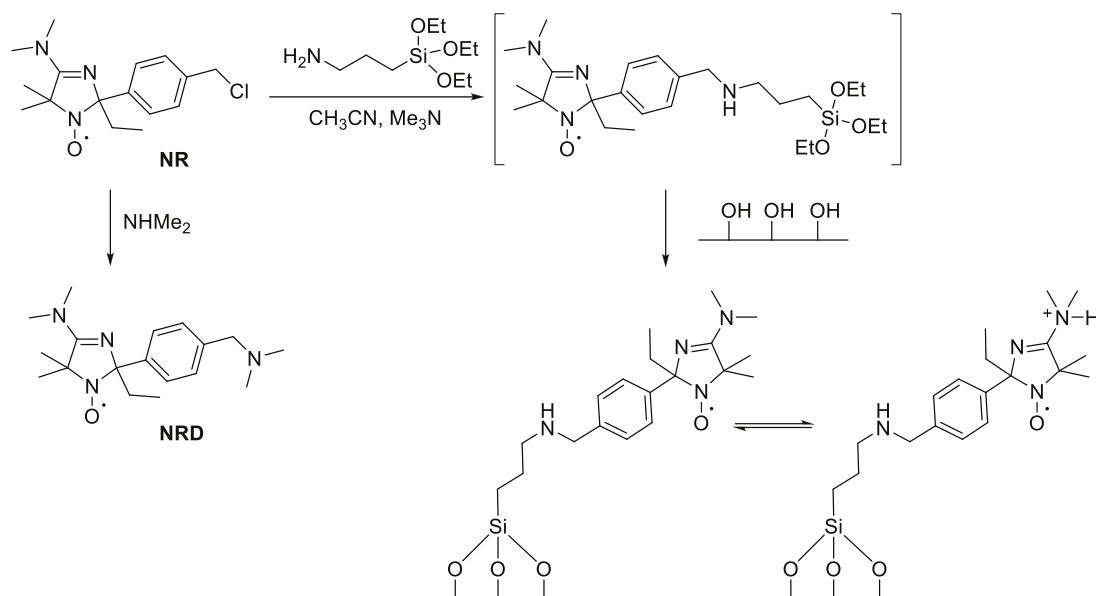
Scheme 1. Synthesis of 4-dimethylamino-2-(4-(dimethylaminomethyl)phenyl)-2-ethyl-5,5-dimethyl-2,5-dihydro-1*H*-imidazole-1-oxyl (NRD) and surface modification of AAO with an adduct of 4-dimethylamino-5,5-dimethyl-2-(4-(chloromethyl) phenyl)-2-ethyl-2,5-dihydro-1*H*-imidazol-1-oxyl hydrochloride semi-hydrate (NR) and aminopropylethoxysilane (APTES). See text for experimental details.

was 1:250 g/ml. The concentration of NR in solutions was kept at or below 0.5 mM in order to avoid additional broadening the EPR spectra by interspin dipolar and/or spin exchange interactions. *p*H was adjusted with 0.1 M HCl or NaOH and the ionic strength, *I*, to 0.1 M with NaCl. Prior to the experiments the AAO strips were immersed into NR solutions for at least 7–10 min to establish equilibrium between the external bulk solution and the aqueous phase inside the nanopores (*i.e.*, internal solution). Thereafter, *p*H-values of the equilibrium external bulk solutions, pH_{ext}, were measured by a 3-in-1 combination *p*H electrode and a Mettler Toledo FP20 *p*H meter (Mettler-Toledo, Columbus, OH, USA) with the specified accuracy of ±0.01 *p*H unit. The ±0.01 *p*H unit error was significantly less than the typical errors of ±0.05 *p*H units arising from the analysis of EPR titration curves and, therefore, were neglected.

Potentiometric titration of AAO membranes has been carried out by a conventional batch multi-sample technique [61,62].

2.5. EPR experimental procedures

All EPR spectra were recorded at room temperature (≈293 K) using X-band CW Bruker Elexys E500 EPR spectrometer equipped with a Super Jigh Sensitivity Resonator (Bruker BioSpin, Billerica, MA, USA). Aqueous solutions of NR were drawn into open end quartz capillaries with *i.d.* = 0.50 mm and *o.d.* = 0.70 mm (VitroCom Inc., Mountain Lakes, NJ, USA), the ends of the capillary were sealed with Critoseal® (Leica Microsystems Inc., Buffalo Grove, IL), and placed in a standard quartz EPR tube (*i.d.* = 3.0 mm). The tube was consequently inserted into the EPR resonator.

For EPR experiments with nanoporous substrates the AAO strips (3 mm × 8 mm) were soaked with an aqueous solution of NR for at least 7–10 min. After removal of a strip from the solution an excess of liquid outside the AAO substrates was removed with a filter paper, the strip was inserted into a quartz EPR tube (*i.d.* = 3.5 mm), and EPR spectra were recorded immediately thereafter. Enclosing the samples in the quartz tube prevented water evaporation from the nanopores. The samples were examined visually before and after the recording the EPR spectra to ensure that the nanopores remained filled with the NR solutions. Further details of EPR titration experiments and analysis of EPR spectra are given elsewhere [44,45,63].

The experimental EPR procedures with AAO-2 containing NR

covalently attached to the inner pore surfaces were the same except the external aqueous solution did not contain NRD.

3. Results and discussion

3.1. Characterization of nanoporous AAO membranes

Fig. 1 shows representative SEM images of the back sides of four nanoporous AAO membranes fabricated for this study. The images demonstrate a hexagonally ordered pore morphology that is typical for the two-step anodization procedure [3]. The size of the individual ordered domains is likely related to the crystalline domains present in the aluminum foil which was used as the starting material for the anodization. The pore diameters were analyzed directly from these images using in-house developed Matlab script but discarding sections of the images that were visually distorted by SEM charging artifacts. From this analysis it was found that the pore enlargement procedure employed for tuning the pore diameter has a negligible effect on the width of the distributions of the pore diameters.

3.2. Rotational motion of spin labels and probes in AAO nanochannels

Fig. 2 shows representative EPR spectra of *p*H-sensitive nitroxide radical NR when introduced as an aqueous solution of NaCl (*I* = 0.1 M ionic strength) into AAO nanochannels (A) and when the nitroxide was covalently attached to the inner AAO pore surface using silane chemistry (see Scheme 1) and the nanopores were soaked with NaCl aqueous solution of the same ionic strength (B, C). The sharp three-line spectrum (Fig. 2A) is characteristic of a nitroxide in a fast rotational motion regime [64] and, therefore, is attributed to the nitroxide in the aqueous phase confined within the nanopores. Some small asymmetry in the high field nitrogen hyperfine component is indicative of the two coexisting forms of the nitroxide (*i.e.*, R and RH⁺) when *p*H of the external bulk solution was $pH_{ext} = 5.60$.

The shape of Fig. 2A EPR spectrum indicates that the rotational diffusion of NR in the nanopore aqueous phase is significantly affected by the nano confinement. Specifically, the corresponding rotational correlation time increases from $\tau_c \approx 10^{-11}$ s observed for the bulk aqueous phase (spectra are not shown) to $\tau_c \approx 2 \times 10^{-10}$ s when inside
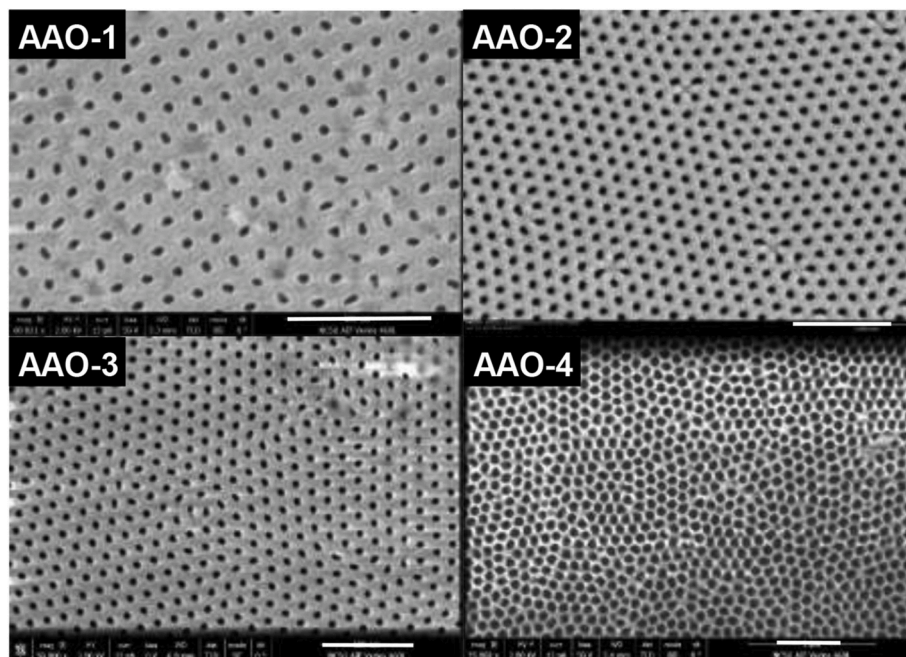
Fig. 1. SEM images of the back sides of anodic aluminum oxide (AAO) membranes with different pore diameters, d, fabricated at NCSU for this study: AAO-1, $d = 31 \pm 4$ nm; AAO-2, $d = 37 \pm 3$ nm; AAO-3, $d = 39 \pm 3$ nm; AAO-4, $d = 71 \pm 8$ nm. The images were taken at different magnifications indicated by a white bar of 500 nm in width at the bottom of each image.

the AAO nanochannels. This significant about 20-fold increase in τ_c could be related to changes in the effective viscosity of water in the nanochannels and/or some transient (on the EPR time scale) interactions of the NR with the nanochannel inner surfaces. Even though the rotational correlation time undergoes a large change, the nanoconfinement has no measurable effects on the isotropic nitrogen hyperfine coupling constants, a, for either the protonated and nonprotonated forms of the radical when compared to the bulk aqueous phase: these constants remain the same within the accuracy of the experiment (see Fig. 3). It should be noted that the parameter a is a sensitive reporter of the local solvent polarity [65,66] and even more the hydrogen bonding between the nitroxide NO$^\bullet$ moiety [67,68]. Therefore, such an EPR observation is indicative of negligible effects of nanoconfinement on the effective polarity of the aqueous phase.

Covalent attachment of NR to the inner surfaces of the AAO channels is expected to significantly slow the rotational dynamics of the nitroxide. Indeed, all EPR spectra measured from such samples (see Fig. 2B and C) were found to be broader and corresponded to an intermediate motion regime. The spectra measured at pH$_{ext} \geq 4.0$, such as the one shown Fig. 2C, reveal the coexistence of at least two components characterized by different rotational correlation times. For example, simulation modelling of the spectrum Fig. 2C measured at pH$_{ext} = 5.95$ using isotropic rotational diffusion model [64] yields two components with $\tau_{c1} \approx 2.0 \times 10^{-9}$ s (Signal 1, Fig. 2D) and $\tau_{c2} \approx 3.5 \times 10^{-8}$ s (Signal 2, Fig. 2E). By measuring the signal intensities from digital double integration of the corresponding EPR spectra, the fractions of the two signals were $\approx$14% and $\approx$86%, respectively. We note that similar two-component EPR spectra but with closer values of the rotational correlation times, τ_c, were previously observed for nitroxide radicals covalently attached to SiO$_2$ surfaces [69].

The two-component EPR spectra characterized by different rotational correlation times are likely to be attributed to different locations of the spin labels at the nanochannel surface. We hypothesize that the Signal 1 characterized by the shorter correlation time $\tau_{c1} \approx 2.0 \times 10^{-9}$ s (Fig. 2D) originates from the spin labels covalently attached to the nanochannel surface via a tether which still has a high degree of flexibility (see also Scheme 1). When extended into an aqueous phase, such a

tether is expected to provide for a nearly isotropic rotational diffusion of the nitroxide albeit at a rate significantly slower than the one observed for the spin probe freely diffusing in an aqueous phase. It is hypothesized that a nitroxide covalently attached to the nanochannel surface could be further immobilized, at least transiently, by forming a hydrogen bond between the hydrogen atom of the hydroxyl surface groups and the nitrogen atom of the spin label imidazole ring. Such an immobilized nitroxide is characterized by a longer rotational correlation time $\tau_{c2} \approx 3.5 \times 10^{-8}$ s and could be assigned to the Signal 2 of Fig. 2E. Formation of a hydrogen bond between the pyridine nitrogen atom and the hydroxyl group on Al$_2$O$_3$ surface has been previously discussed by several authors (e.g. Ref. [70,71]).

For simulations of intermediate and slow motion EPR spectra, such as one shown in Fig. 2C, using software described in Ref. [64], the values of the principal components of the nitrogen hyperfine coupling tensor $\boldsymbol{A}$ were adjusted and then the isotropic nitrogen hyperfine coupling constant, a, was calculated as:

$$a = \frac{1}{3}\left(A_x + A_y + A_z\right) \tag{1}$$

For example, for the spectrum measured at pH$_{ext} = 5.95$ (Fig. 2C) the calculated values of a for the two components were found to be $a_1 \approx 15.38$ G (Signal 1) and $a_2 \approx 14.96$ G (Signal 2). The first value $a_1 \approx 15.38$ G is essentially the same as a(R) = 15.44 $\pm$ 0.05 G observed for this spin probe in the non-protonated form (Table 1) while the second value $a_2 \approx 14.96$ G falls in between a(R) = 15.44 $\pm$ 0.05 G and a (RH$^+$) = 14.60 $\pm$ 0.05 G observed for this radical in non-the protonated and protonated forms, respectively.

EPR spectral lineshape changes indicated that the rotational dynamics of NR attached to nanochannel surfaces changes significantly with a gradual decrease in pH$_{ext}$ below 4 pH units (for representative spectra see Fig. 2). Initially, the fraction of a more mobile Signal 1 decreases. Secondly, upon a further decrease in pH the contribution of the immobilized Signal 2 starts to decrease and then these two components are replaced by the Signal 3 (Fig. 2B) characterized by a shorter rotational correlation tine $\tau_{c3} = 5 \times 10^{-10}$ s and the isotropic nitrogen hyperfine coupling constant $a_3 \approx 14.52$ G. At pH$_{ext} = 2.58$ least squares
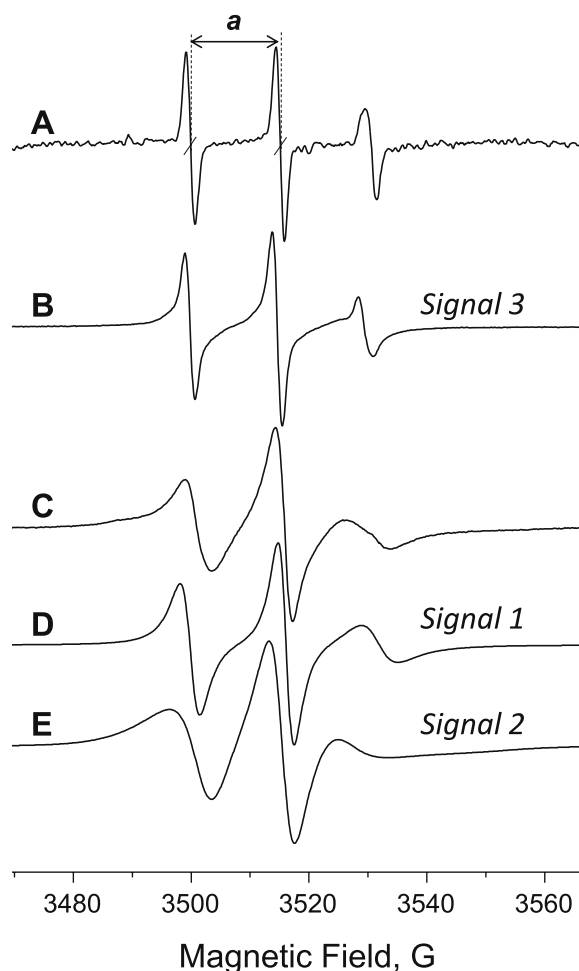
Fig. 2. Room temperature X-band (9 GHz) EPR spectra of nitroxide NR from an aqueous phase confined in untreated AAO-2 nanopores ($d \approx 37$ nm) (A) and NR covalently attached to the inner pore surfaces (B, C) of the same AAO-2 and soaked in an aqueous solution of NaCl ($I = 0.1$ M) and pH adjusted with 0.1 M HCl or NaOH to pH$_{ext}$ = 5.60, 2.58, 5.95, respectively. The arrows and dashed lines in the spectrum (A) illustrate measurements of an isotropic nitrogen hyperfine coupling parameter a as a splitting between the low and the central magnetic field nitrogen hyperfine components; such a splitting was employed to quantify the nitroxide protonation state. EPR spectra (D) and (E) are results of the least-squares simulations of the spectrum (C) into two components (*Signal 1* and *Signal 2*) using software developed by Freed and coworkers [64]. The fractions of the *Signal 1* and *Signal 2* were 14% and 86%, respectively, based on the calculated values of the corresponding double integrals. The spectrum (B) is assigned to the fully protonated form of the nitroxide (*i.e.*, RH$^+$, *Signal 3*) covalently attached to the nanochannel surface. All spectra are normalized by the peak-to-peak amplitude. See text for details.

simulations of the experimental EPR spectra (not shown) reveal no *Signal 1* but a superposition of the *Signal 2* ($\approx$75% of the total double integrated intensity) and the *Signal 3* ($\approx$25%). The magnitude of the isotropic nitrogen hyperfine coupling constant $a_3 = 14.52 \pm 0.10$ G coincides within the experimental error with $a = 14.54 \pm 0.05$ G measured for the protonated form of the radical NRD (Table 1). We note here that the reaction of NR with aminopropylethoxysilane causes a change in the side chain and, therefore, the isotropic nitrogen hyperfine coupling constants measured for the NR covalently attached to the alumina surface should be compared with those measured not for solutions of NR but for NRD, which is a closer water-soluble analogue of this spin label (see Scheme 1).

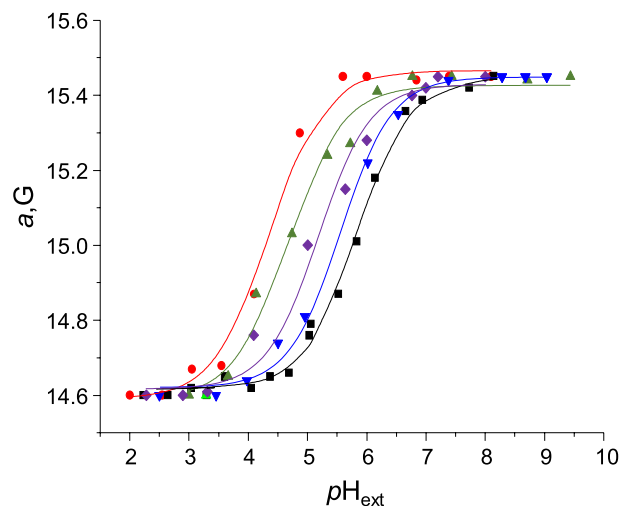From the comparison of isotropic nitrogen hyperfine coupling

Fig. 3. Experimental room temperature EPR titration curves obtained by plotting isotropic nitrogen hyperfine coupling constant a *vs.* pH$_{ext}$ for aqueous solutions of nitroxide NR in a bulk aqueous phase at ionic strength $I = 0.1$ M (black squares) and confined inside the nanochannels of AAO-1 (red circles), AAO-2 (green triangles), AAO-3 (magenta diamonds), AAO-4 (blue triangles) membranes with the average pore diameters $d \approx$ 31, 37, 39 and 71 nm, respectively. The best fits to the modified Henderson-Hasselbalch equation are shown as solid lines of the same color as the corresponding symbols and parameters are summarized in Table 2. Errors of the individual measurements of a for NR in the bulk aqueous phase are ±0.02 G while for NR confined inside AAO those values are ±0.04 G. Errors of pH$_{ex}$ are ±0.01 of pH units. (For interpretation of the references to color in this figure legend, the reader is referred to the Web version of this article.)

constants, we conclude, that the *Signal 3* corresponds to the spin label NR in the protonated form (*i.e.*, RH$^+$). With a decrease in pH an increase in concentration of the hydrogen ions in the surface layer ensures breaking the hydrogen bond formed between the nitrogen of the imidazole ring and the hydroxyl groups of the surface. This is accompanied by a decrease in the fraction of the *Signal 1* and a transition of the radical into the fully protonated form (*Signal 3*). The rotational diffusion of the covalently bound positively charged nitroxide in the protonated form (*i.e.*, RH$^+$) increases due to an electrostatic repulsion from the positively charged alumina surface: compare the corresponding $\tau_{c3} = 5 \times 10^{-10}$ s with $\tau_{c1} = 2 \times 10^{-9}$ s observed for the non-protonated form of NR. It is worthwhile to note here that the protonation of the secondary amine in the tether attaching the nitroxide to the surface (see Scheme 1) is unlikely to play any role in the observed effects because its pK_a is expected to be outside the pH range of EPR titrations based on the known correlation of the base strengths of amines [72]. Furthermore, only one $pK_a = 5.76 \pm 0.05$ was observed in the EPR titration of the model compound NRD (Table 1 and Fig. S2 of the Supplemental Information).

3.3. EPR titration of nitroxides in AAO nanochannels prepared without annealing

Average acidity inside the AAO nanopores was determined from measuring EPR spectra of AAO strips soaked with NR dissolved in water. Isotropic nitrogen hyperfine splitting was measured as a distance between the low magnetic field and the central nitrogen hyperfine components (see Fig. 2A) and plotted as a function of pH. Fig. 3 compares the obtained EPR titration curves for the AAO nanopores of different diameters and the calibration titration curve measured for the same NR in a bulk aqueous solution (black squares). It was found that all the titration curves for NR in nanopores are shifted to the lower pH values relative to the calibration curve shown as a black line (Fig. 3). As further elaborated in the preceding studies of fluorescent [73,74] and EPR pH-sensitive probes [44,51], the observed pK_a^{loc} of a molecular

probe is determined by the additive contributions of (*i*) intrinsic pK_a^0 of the spin probe, (*ii*) ΔpK_a^{ch} arising from a change in the Gibbs free energy upon transferring the probe from the bulk aqueous water phase to water confined inside the nanochannels, ΔG_{ch}, and (*iii*) ΔpK_a^{el} contribution from the local electric potential, Ψ:

$$pK_a^{loc} = pK_a^0 + \Delta pK_a^{ch} + \Delta pK_a^{el} \quad (2)$$

where:

$$\Delta pK_a^{el} = -e\psi/\ln(10)kT \quad (3)$$

Assuming that ΔpK_a^{ch} is negligible, the shifts of the titration curves to lower pH (Fig. 3) indicate a positive local electric potential Ψ arising from the nanochannel surface charge. Thus, the inside surfaces of AAO nanochannels must be positively charged at $pH < 7$ – the range covered by the pH-sensitive EPR probe NR employed in this work. Previously, the positive charge of the γ-Al$_2$O$_3$ surface in the acidic-to-normal range has been established experimentally by potentiometric titration [75]. Specifically, the positive surface charge was found to decrease with increasing pH of the bulk solution till reaching the point of zero charge (*pzc*) at $pH \simeq 7.63$ (at temperature of 20 °C) and turning negative with a further increase in pH [75]. Other literature data for *pzc* and isoelectric points (*iep*) obtained by potentiometric titration and streaming potential measurements for α- and γ-Al$_2$O$_3$ and the outside surfaces of the AAO membranes all indicated *pzc* values close $pH = 9.0 \pm 0.8$ [76–80]. Thus, the positive surface charge of the AAO nanochannels reported by the nitroxide NR at $pH < 7.0$ is consistent with the interfacial properties of amorphous Al$_2$O$_3$ or γ-Al$_2$O$_3$ exposed to water. This is expected for the membranes subjected to annealing at 700 °C after the fabrication; based on literature data this temperature is insufficient to convert the surface of the channels into α-Al$_2$O$_3$ [81].

A decrease in diameter of the AAO nanochannel channels progressively shifts the EPR titration curves to lower pH values *vs.* the calibration curve for the bulk solution (see Fig. 3). This shift is characterized by changes in the observed pK_a^{loc} (Table 2) determined by least-squares fitting the data to a modified Henderson-Hasselbalch equation [82]:

$$a = \frac{a(R) \cdot 10^{(pH - pK_a^{loc})} + a(RH^+)}{1 + 10^{(pH - pK_a^{loc})}} \quad (4)$$

The observed decrease in the apparent pK_a^{loc} values indicates that the effective acidity within the AAO nanochannels, pH^{ch}, reported by the nitroxide is higher than pH^{ext} measured for the initially equilibrated bulk aqueous phase. The observed shift in the spin probe pK_a, *i.e.*, $\Delta pK_a = pK_a^{loc} - pK_a^0$, starts from 0.25 ± 0.08 pH units for the largest ≈ 71 nm nanochannels (AAO-4) and reaches 1.48 ± 0.08 pH units for the smallest ≈ 31 nm channels (AAO-1) studied here (Table 2).

According to eq. (2), two factors, ΔpK_a^{ch} and ΔpK_a^{el}, are expected to affect pK_a^{loc} values measured by the spin probe. The first factor, ΔpK_a^{ch}, accounts for a change in the Gibbs free energy upon transferring the

probe molecule from a bulk aqueous phase to a water volume confined inside the nanochannels. The AAO nanochannels exhibit an exceptionally high length-to-diameter ratio readily exceeding 1,000 in our nanoporous membranes. Therefore, the water structure in such long channels of a nanoscale diameter could be somewhat different from that of the bulk, thus, contributing to the observed deviation of pH^{ch} from pH^{ext} [61,62,83]. However, while rotational diffusion of the nitroxide NR in AAO nanochannels was significantly slower *vs.* that in the bulk aqueous phase (corresponding $\tau_c \approx 2 \times 10^{-10}$ s *vs.* $\tau_c \approx 10^{-11}$ s), the values of the isotropic nitrogen hyperfine coupling constant a for either R or RH$^+$ forms of the nitroxide were essentially unaffected by the nanoconfinement as demonstrated by about the same plateaus for the hyperfine parameter a in all the EPR titration curves shown in Fig. 3. The parameter a is known to be primarily affected by the formation of hydrogen bonds between a donor molecule (e.g., water) and the ntroxide N–O$^\bullet$ moiety [68,84]. From these considerations the effects of an altered water structure due to nanoconfinement is likely to be small for these relatively large (*i.e.*, $d \geq 31$ nm) pores. Then one could argue that the observed longer values of rotational correlation time τ_c in the nanochannels are likely to be caused by transient interactions of the spin probe with the nanochannel surfaces under conditions that the EPR spectra are still in the fast exchange regime.

The second factor contributing to the observed shift in the probe pK_a is the ΔpK_a^{el} term arising from a local electric potential, Ψ (eq. (3)). As already discussed above, at $pH < 7.0$ the alumina surface is expected to be positively charged and the related electric potential would shift the probe pK_a to lower pH values. Because the surface potential is screened by the counter ions, the effect would be more pronounced for the probes located within a surface layer with a thickness d comparable to the Debye length ($\chi^{-1} \approx 0.96$ nm for an aqueous solution of 0.1 M ionic strength) and then it would rapidly decay towards the pore center [43]. If we assume that the surface electrostatic potential shifts the spin probe pK_a only within the thin layer with the thickness d adjacent to the surface of a cylindrical pore of a radius R, then the volume fraction of such a layer is given by $2d/R$, when $d \ll R$. The latter condition is always satisfied in our experiments because $d \approx \chi^{-1} \approx 0.96$ nm and $R > 15$ nm. The nitroxide EPR spectrum appears to be in the fast exchange limit (the observed single-component EPR spectra at high and low pH values when the nitroxide NR exists in a single protonation state probe (not shown) justifies this assumption), and therefore, for the spin probe rapidly diffusing in and out the surface layer the shift in ΔpK_a^{el} should be averaged out and, therefore, the observed pK_a^{loc} is expected to decrease as $1/R$ in accord with the experimentally observed trend (see Table 2). We note, however, that according to calculations based on the Poisson−Boltzmann double layer theory and typical values of the surface potentials, the effects of the surface potential on the pK_a value of a freely diffusing nitroxide should be negligibly small for the pores larger than *ca.* 10 nm in diameter (see our ref. [43]). Then, the reliably measured shifts in the NR pK_a^{loc} values observed for the pores as large as 71 nm (Table 2) could indicate that the spin probe NR is primarily residing next to the surface double layer. This would also be in the agreement with the changes in the rotational correlation time τ_c we observed and discussed above.

3.4. Effect of annealing on electrostatic properties of AAO nanopores

Typically, the presence of the surface groups undergoing protonation at a specific pK_a value and act as buffers would manifest in an appearance of a horizontal plateau in the experimental EPR titration curves. For example, such plateaus were observed for EPR titrations of carboxyl functional groups present on the surface of a cation ion exchange resin KB-2 [61] and also silanol groups for SiO$_2$ powder [62] and SBA-15 or MCM-41 mesoporous molecular sieves [85]. However, no such plateaus have been observed for EPR titration of the spin probe NR in all the AAO nanochannels studied here and not subjected to the annealing above

Table 2
Average pore diameter, d, of AAO membranes, pK_a^{loc} of aqueous solutions of NR in bulk phase and when confined in AAO nanochannels, and the corresponding ΔpK_a shifts *vs.* pK_a^0 in bulk water from EPR titration curves at room temperature.

Sample	Average pore diameter, d, nm	pK_a^{loc}	$\Delta pK_a = pK_a^{loc} - pK_a^0$
Bulk water	n/a	5.82 ± 0.05^c	0
AAO-1	31 ± 4^b	4.34 ± 0.07^c	-1.48 ± 0.08
AAO-2	37 ± 3^b	4.87 ± 0.07^c	-0.95 ± 0.08
AAO-3^a	39 ± 3^b	5.20 ± 0.07^c	-0.62 ± 0.08
AAO-4	71 ± 8^b	5.57 ± 0.07^c	-0.25 ± 0.08

[a] Before the annealing above 700 °C.
[b] Standard errors were derived from analysis of the experimental SEM images.
[c] Standard errors were derived from least squares fitting of EPR titration curves.

700 °C (see Fig. 3) at least within the *p*H sensitivity range of this radical (*i.e.*, from 4.9 to 6.9 *p*H units). The surface of the pores of as-prepared AAO is known to be formed by an amorphous alumina [54] with the coordination environment of the aluminum atoms considered to be closely related to γ-Al$_2$O$_3$ [2]. For γ-Al$_2$O$_3$ dissociation of the protonated surface hydroxyl groups AlOH$_2^+$ $\rightleftharpoons$ AlOH + H$^+$ occurs at *p*K$_a$ ranging from 5.3 to 6.2 *p*H units [86]. Thus, the absence of such plateaus in the titration curves shown in Fig. 3 indicates that the surface chemistry of the nanochannels of the AAO membranes after annealing at 700 °C differs from that of γ-Al$_2$O$_3$ powder and, apparently, still remains amorphous like in as-anodized AAO. Indeed, previous ^{1}H and ^{27}Al NMR studies of high-surface-area alumina powders indicated a dehydration by a condensation of both Al$_2$OH and AlOH groups to form distorted, hydrogen-bearing 4-, 5-, and 6-coordinate aluminum-containing intermediates upon heating in the 350–500 °C range [87].

Among many crystalline phases of Al$_2$O$_3$ (α, χ, η, δ, κ, θ, γ, ρ) mesoporous γ-Al$_2$O$_3$ is most widely utilized for both catalytic applications and as a versatile sorbent material because of a favorable combination of morphological properties such as surface area, pore volume, and pore size as well as acid-base characteristics [88,89]. The γ-phase of alumina is typically formed by a dehydration of aluminum oxyhydroxide boehmite upon heating to temperatures from 400 to 700 °C [88]. The phase is representative of transitional Al$_2$O$_3$ with a disordered crystalline structure that could be further transformed upon an additional heating. The heating of γ-Al$_2$O$_3$ leads to a series of polymorphic transformations from a highly disordered cubic close-packed lattice to a more ordered cubic close-packed θ-Al$_2$O$_3$. Further heating to *ca.* $T = 1,200$ °C causes θ-Al$_2$O$_3$ to undergo a reconstructive transformation by nucleation and growth, during which the oxygen atoms rearrange into a hexagonal close-packed structure to form a thermodynamically stable α-Al$_2$O$_3$ phase, which is the final product of thermal or dehydroxylation treatments of all the aluminum hydroxides [88]. Thus, we expect that annealing of AAO would also result in significant changes in the nanopore surface properties and affect the protonation equilibria of the molecules inside the pores.

In accord with such expectations, EPR titration curves for the radical NR were found to change significantly after annealing the AAO-3 membranes at 900 and then 1,200 °C (Fig. 4). The most significant change is the appearance of plateaus at *p*H$_{ext}\approx$6.0–8.2 (Fig. 4). This *p*H range is consistent with titration of AlOH$_2^+$ surface groups that would act as a buffer [86]. This is in the full agreement with a formation of γ-Al$_2$O$_3$ transition phase in the skeleton regions of the membrane and also some nanocrystalline regions of α-Al$_2$O$_3$ throughout the structure upon heat treatment to 900 °C as was previously reported by McQuaig et al. based on bright-field TEM and diffraction studies [53]. We note that the width of the plateau for AAO-3 annealed at 1,200 °C is significantly smaller than the one observed for the sample heat-treated to 900 °C (Fig. 4). This could serve as an indication of a fraction of the γ-Al$_2$O$_3$ transition phase present. Indeed, the further annealing of AAO at 1,200 °C was shown to completely transform the material to the stable α-Al$_2$O$_3$ structure [53].

The EPR titration curves for the spin probe NR also differ considerably for the 900 and 1,200 °C annealed AAO and when compared with the 700 °C annealed and as-anodized AAO-3 (Figs. 3 and 4). Specifically, the titration curve for AAO-3 annealed at 1,200 °C is shifted to higher *p*H values *vs.* either the curve for the membrane annealed at 900 °C or the calibration curve measured for NR in the bulk aqueous phase. The shift direction of the former two curves *vs.* the calibration is opposite to the one observed for all the other AAO samples annealed at 700 °C. In accord with eqs. (2) and (3) this observation indicates a switch in the surface charge from positive for the AAO-3 annealed at 700 °C to negative (AAO-3 annealed at 1,200 °C) at *p*H > 8. The negative surface charge is typical for a crystalline α-Al$_2$O$_3$ phase (*i.e.*, corundum) at this *p*H range [90]. Previously, a phase transition leading to a formation of α-Al$_2$O$_3$ on the surface of the AAO nanochannels upon high temperature annealing has been reported by several authors [53,57,91]. The latter
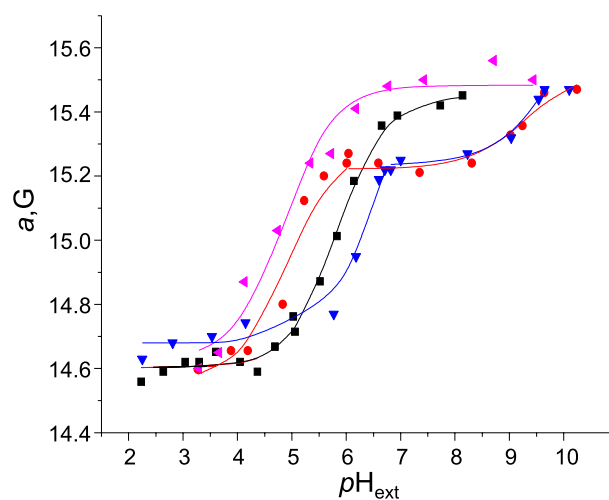

Fig. 4. Experimental room temperature EPR titration curves obtained by plotting isotropic nitrogen hyperfine coupling constant *a vs.* *p*H$_{ext}$ for aqueous solutions of the nitroxide NR in a bulk aqueous phase at ionic strength $I = 0.1$ M (black squares) and reporting on the average acidity inside the nanochannels of AAO-3 membrane annealed at 700 °C (magenta triangles), 900 °C (red circles) and 1,200 °C (blue triangles). The best fits to the modified Henderson-Hasselbalch equation are shown as solid lines of the same color as the corresponding symbols. Errors of the individual measurements of *a* for NR in the bulk aqueous phase are ± 0.02 G while for NR confined inside AAO those values are ± 0.04 G. Errors of *p*H$_{ex}$ are ± 0.01 of *p*H units. (For interpretation of the references to color in this figure legend, the reader is referred to the Web version of this article.)

and other studies [92] also revealed that such an annealing causes a moderate increase in the diameters and changes in the nanochannel morphology. Specifically, it was observed that the pores would become wider but also slightly deformed and less circular in shape [53]. Another, perhaps, even more likely reason for the observed shift is a decrease in the surface charge associated with a decrease in the number of the Lewis acid sites (non-lattice aluminum cations) – an effect that was previously observed by NMR in a course of the annealing studies [87]. Finally we note that for AAO-3 annealed at 1,200 °C at *p*H < 6 the EPR titration curve is not running parallel to the calibration curve for the NR in the bulk aqueous phase and that these curves intersect at *p*H$_{ext}\approx$5 (Fig. 4). This agrees well with our previous observation of the effective value of the zero charge point *pzc*$_{eff} \approx$4.7 of *p*H units for the inner surfaces of the AAO nanochannels [44].

3.5. Surface potential AAO nanopores from EPR titration of a covalently attached nitroxide

The chlorophenyl moiety of NR provided for a covalent attachment of this EPR molecular *p*H-sensor to aminopropylethoxysilane and the inner surfaces of the nanochannels (Scheme 1) so this water-soluble spin probe could also be employed as a spin-label in which the *p*H-reporting moiety is positioned close to the nanochannel surface. The apparent *p*K$_a$ value of such a covalently bound label was found to be strikingly different from *p*K$_a$ of the NR probe diffusing in the nanochannels (Fig. 5). We note, however, that the reaction of the NR chlorophenyl moiety with the primary amine of aminopropylethoxysilane could also potentially affect *p*K$_a^0$ of the nitroxide. In order to evaluate the magnitude of such effect we have synthesized a model compound NRD by reacting NR with dimethylamine (see 2.2 of the Experimental Section). The resulting molecule is water soluble and has a side chain closely mimicking one for the surface-tethered nitroxide. Experimental EPR titration of NRD indicated that the *p*K$_a^0$ value of this molecule is essentially the same as that of NR; there was a small effect on the isotropic nitrogen hyperfine coupling constant *a* (RH+) of the nitroxide in the protonated form
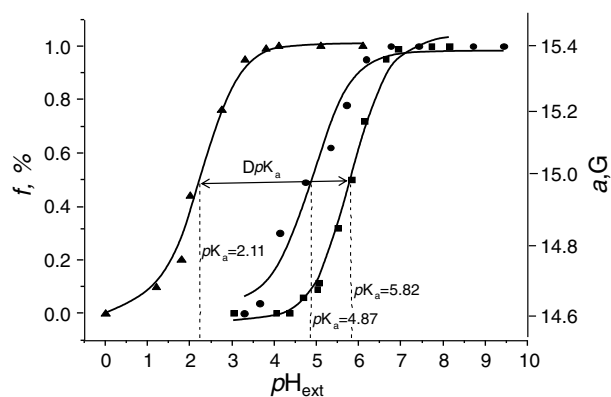
Fig. 5. Experimental room temperature EPR titration curves for aqueous solutions of spin probe NR in a bulk volume (filled squares) and inside the AAO-2 nanochannels ($d = 37 \pm 3$ nm, filled circles) as derived from the isotropic nitrogen hyperfine coupling constant a measured for the fast motion nitroxide component (see Fig. 2A). EPR titration curves derived from least-squares fitting of the first derivative EPR spectra of NR covalently attached to the wall of AAO-2 nanochannels (*i.e.*, when NR was employed as a label) to calculate the fraction f of the slow motion component are shown as filled triangles. All EPR titrations were carried out in a solution of $I = 0.1$ M ionic strength. The best fits to the modified Henderson-Hasselbalch equation are shown as solid lines. Dashed lines indicate apparent pK_a values. Errors of the individual measurements of a for NR in the bulk aqueous phase are ± 0.02 G while for NR confined inside AAO those values are ± 0.04 G. Errors in f are ± 0.02. Errors of pH_{ex} are ± 0.01 of pH units.

(Table 1 and Fig. S4) due to the altered side chain on NRD. Thus, the EPR titration data for NR covalently attached to the alumina surfaces could be directly compared with those measured for NR diffusing within the nanopores.

Analysis of the EPR titration curves shown in Fig. 5 revealed that for AAO-2 ($d \approx 37$ nm) the apparent pK_a of the covalently attached NR label was 2.11 ± 0.04 of pH units whereas for the probe diffusing in nanopores $pK_a = 4.87 \pm 0.07$. Such a significant decrease in the apparent pK_a values ($\Delta pK_a = -2.76 \pm 0.08$) is related to the effect of a large positive electrostatic potential of the pore surface that is not effectively screened by the counter ions at the location of the covalently attached NR. However, for the NRs diffusing inside the nanopores, at ionic strength of $I = 0.1$ M the ion double layer formed next to the pore surface is expected to fully screen the surface electrostatic potential for all the pore diameters studied here. Indeed, recent calculations based on the Poisson−Boltzmann double layer theory and a comparison with the experiment have shown that for long cylindrical pores with $d \approx 8$ nm or larger the EPR pH probe freely diffusing inside the pores and satisfying fast exchange conditions would be insensitive to typical values of surface potential (*i.e.*, $\psi < 200 - 300\, mV$) at room temperature and $I = 0.1$ M [43]. From these considerations, the value of $pK_a^{loc} = 4.87 \pm 0.07$ for the unattached NR probe could be taken as the nitroxide pK_a values at $\psi = 0$ and the observed $\Delta pK_a = -2.76 \pm 0.08$ shift should be attributed to ΔpK_a^{el}. Then, from eq. (3) the magnitude of the electrostatic surface potential at the probe is $\psi = +163 \pm 5$ mV. The latter is a consertvative estimate. Indeed, as discussed above, the NR diffusing inside the AAO nanochannels could be transiently interacting with the pore surfaces and, if so, it would be effectively located in the area with non-negligible electrostatic potentioal. Then the $pK_a = 5.82 \pm 0.05$ value for NR in the bulk aqueous solution could be taken at the reference point for $\psi = 0$ V. Using the latter refernce point, the magnitude of the electrostatic surface potential at the location of the attached probe is $\psi = +219 \pm 5$ mV.

It is well known that the values of the surface charge density, σ, and the zeta potential, ζ, measured by electrokinetic or potentiometric titration methods depend on the nature of the electrolyte, ionic strength I of the solution, pH_{ext}, and temperature. Previously, several values of

zeta potential ranging from $\zeta \approx +30$ to $+100$ mV have been reported for γ-Al_2O_3 surfaces at $pH_{ext} = 5$ depending on I and the nature of the electrolyte [86,87,93]. However, ζ potential is measured at the location of the so-called slip plane, which could be further away from the surface than the covalently attached NR we employed to measure pH_{loc}. By taking conservative value of $\psi = +163 \pm 5$ mV at the location of the pH-sensitive spin label, typical values of $\zeta \approx +30$ mV, and using the Debye – Hückel equation with $I = 0.1$ M, $T = 298$ K under an assumption of a uniform surface charge [75], we estimate that the slip plane is located by ≈ 0.5 nm further away from the covalently attached NR.

4. Conclusions

Continuous wave X-band EPR spectroscopy of a pH-sensitive nitroxide radical employed as either (*i*) a freely-diffusing spin probe or (*ii*) a covalently-attached spin label has been used to study acid-base equilibria in the pores and surfaces of ordered nanoporous anodic aluminum oxide (AAO) membranes prepared by a two-step anodization process. It was shown that by changing the average pore diameter from $d \approx 31$ to ≈ 71 nm one can vary the acidity of the aqueous medium inside the nanochannels. Even larger effects on local acidity and the surface charge could be achieved by annealing the AAO membranes first to 900 and then to 1,200 °C. While as-prepared the surface of AAO nanochannels is positively charged due to the amorphous nature of the Al_2O_3 surface layer, annealing the membranes at 1200 °C inverts the sign of the surface charge to a negative one based on the large shifts of the EPR titration curves. These shifts are in agreement with the consecutive transformations of amorphous Al_2O_3 to γ-Al_2O_3 and then to crystalline α-Al_2O_3 upon annealing at increasing temperatures. The latter phase transformations provide for a switch in the sign of the surface charge from positive to negative. Comparison of the magnitude of the shifts of the EPR titration curves for as-anodized AAO samples studied in this work ($\Delta pK_a \approx 1.48$ for $d \approx 31$ nm pores, Table 2) with $\Delta pK_a \approx 0.27$ measured previously for AAO of essentially the same diameter $d \approx 29$ nm [44] indicates that the charge density in the former is at least fivefold higher. Thus, we conclude that the anodization conditions could also have a profound effect on the surface electrostatic properties of the AAO nanochannels. We also note that the magnitude of the electrostatic potential measured here by EPR of pH-sensitive nitroxides covalently attached to the nanochannel surfaces is very close to those measured for the surfaces of model biological membranes composed from phospholipids [48]. Thus, the surface charges present in the AAO nanochannels and associated electrostatic potentials are expected to provide for rather large effects on function of biomolecules as well as on the nanochannels' catalytic properties.

Taken together, it was shown that by varying the nanoscale pore diameter and, even more importantly, increasing the annealing temperature, the surface charge of the AAO nanochannels could be varied significantly without further, specific chemical modification. Such surface charge tunability, including switching the sign of the surface charge upon annealing, provides a simple yet robust method to tailor these versatile nanomaterials for specific applications that depend on acid-base equilibria.

in the context of State Task of the Institute of Organic Synthesis named after Academician I. Ya. Postovsky of the Ural Branch of the Russian Academy of Sciences (Pr. AAAA-A19-119012490006-1).

Declaration of competing interest

We honestly state that all this manuscript or its contents have not been published previously and have no competing financial interest.

CRediT authorship contribution statement

Elena G. Kovaleva: Conceptualization, Methodology, Validation, Formal analysis, Investigation, Writing - original draft, Supervision, Project administration, Funding acquisition. **Leonid S. Molochnikov:** Methodology, Writing - original draft. **Darya P. Tambasova:** Investigation, Formal analysis. **Antonin Marek**: Software, Formal analysis, Data Curation. **Melanie Chestnut:** Resources, Investigation. **Victoria A. Osipova:** Resources, Investigation. **Denis O. Antonov**: Investigation. **Igor A. Kirilyuk:** Resources, Methodology, Investigation, Formal analysis. Writing - original draft. Funding acquisition. **Alex I. Smirnov:** Conceptualization, Methodology, Writing - original draft, Writing - Review & Editing, Supervision, Project administration, Funding acquisition.

Acknowledgements

Appendix A. Supplementary data

Supplementary data to this article can be found online at https://doi.org/10.1016/j.memsci.2020.118084.

References

[1] A.M.M. Jani, D. Losic, N.H. Voelcker, Nanoporous anodic aluminium oxide: advances in surface engineering and emerging applications, Prog. Mater. Sci. 58 (2013) 636–704.

[2] W. Lee, S.-J. Park, Porous anodic aluminum oxide: anodization and templated synthesis of functional nanostructures, Chem. Rev. 114 (2014) 7487–7556.

[3] H. Masuda, K. Fukuda, Ordered metal nanohole arrays made by a two-step replication of honeycomb structures of anodic alumina, Science 268 (1995) 1466–1468.

[4] Y.K. Gun'ko, T.S. Perova, S. Balakrishnan, A.A. Potapova, R.A. Moore, E. V. Astrova, Chemical modification of silicon surfaces with ferrocene functionalities, Phys. Status Solidi a-Appl. Res. 197 (2003) 492–496.

[5] S. Tanvir, J. Pantigny, P. Boulnois, S. Pulvin, Covalent immobilization of recombinant human cytochrome CYP2E1 and glucose-6-phosphate dehydrogenase in alumina membrane for drug screening applications, J. Membr. Sci. 329 (2009) 85–90.

[6] M. Arroyo-Hernandez, J. Perez-Rigueiro, A. Conde, A. Climent, R. Gago, M. Manso, J.M. Martinez-Duart, Characterization of biofunctional thin films deposited by activated vapor silanization, J. Mater. Res. 23 (2008) 1931–1939.

[7] E. Hoque, J.A. DeRose, P. Hoffmann, H.J. Mathieu, Perfluorosilanized aluminum oxide surfaces, J. Surf. Anal. 13 (2006) 178–184.

[8] M. Zhang, Y. Bando, K. Wada, Sol-gel template preparation of TiO2 nanotubes and nanorods, J. Mater. Sci. Lett. 20 (2001) 167–170.

[9] Z. Miao, D. Xu, J. Ouyang, G. Guo, X. Zhao, Y. Tang, Electrochemically induced Sol−Gel preparation of single-crystalline TiO2 nanowires, Nano Lett. 2 (2002) 717–720.

[10] N.I. Kovtyukhova, T.E. Mallouk, T.S. Mayer, Templated surface sol–gel synthesis of SiO2 nanotubes and SiO2-insulated metal nanowires, Adv. Mater. 15 (2003) 780–785.

[11] D. Routkevitch, T. Bigioni, M. Moskovits, J.M. Xu, Electrochemical fabrication of CdS nanowire arrays in porous anodic aluminum oxide templates, J. Phys. Chem. 100 (1996) 14037–14047.

[12] R. Liu, J. Duay, S.B. Lee, Electrochemical formation mechanism for the controlled synthesis of heterogeneous MnO2/Poly(3,4-ethylenedioxythiophene) nanowires, ACS Nano 5 (2011) 5608–5619.

[13] N. Li, X. Li, X. Yin, W. Wang, S. Qiu, Electroless deposition of open-end Cu nanotube arrays, Solid State Commun. 132 (2004) 841–844.

[14] S.-H. Zhang, Z.-X. Xie, Z.-Y. Jiang, X. Xu, J. Xiang, R.-B. Huang, L.-S. Zheng, Synthesis of silver nanotubes by electroless deposition in porous anodic aluminium oxide templates, Chem. Commun. (2004) 1106–1107.

[15] W. Wang, N. Li, X. Li, W. Geng, S. Qiu, Synthesis of metallic nanotube arrays in porous anodic aluminum oxide template through electroless deposition, Mater. Res. Bull. 41 (2006) 1417–1423.

[16] R. Seidel, G.S. Duesberg, E. Unger, A.P. Graham, M. Liebau, F. Kreupl, Chemical vapor deposition growth of single-walled carbon nanotubes at 600 °C and a simple growth model, J. Phys. Chem. B 108 (2004) 1888–1893.

[17] Y. Xia, R. Mokaya, Synthesis of ordered mesoporous carbon and nitrogen-doped carbon materials with graphitic pore walls via a simple chemical vapor deposition method, Adv. Mater. 16 (2004) 1553–1558.

[18] J.W. Elam, D. Routkevitch, P.P. Mardilovich, S.M. George, Conformal coating on ultrahigh-aspect-ratio nanopores of anodic alumina by atomic layer deposition, Chem. Mater. 15 (2003) 3507–3517.

[19] M. Fang, J.C. Ho, Area-selective atomic layer deposition: conformal coating, subnanometer thickness control, and smart positioning, ACS Nano 9 (2015) 8651–8654.

[20] N. Linares, A.M. Silvestre-Albero, E. Serrano, J. Silvestre-Albero, J. Garcia-Martinez, Mesoporous materials for clean energy technologies, Chem. Soc. Rev. 43 (2014) 7681–7717.

[21] A. Banerjee, R. Perez-Castillejos, D. Hahn, A.I. Smirnov, H. Grebel, Micro-fluidic channels on nanopatterned substrates: monitoring protein binding to lipid bilayers with surface-enhanced Raman spectroscopy, Chem. Phys. Lett. 489 (2010) 121–126.

[22] C. Zhang, A.I. Smirnov, D. Hahn, H. Grebel, Surface enhanced Raman scattering of biospecies on anodized aluminum oxide films, Chem. Phys. Lett. 440 (2007) 239–243.

[23] G.E.J. Poinern, N. Ali, D. Fawcett, Progress in nano-engineered anodic aluminum oxide membrane development, Materials 4 (2011) 487–526.

[24] A.J. Chung, Y.S. Huh, D. Erickson, Large area flexible SERS active substrates using engineered nanostructures, Nanoscale 3 (2011) 2903–2908.

[25] A. Santos, T. Kumeria, D. Losic, Nanoporous anodic aluminum oxide for chemical sensing and biosensors, Trac. Trends Anal. Chem. 44 (2013) 25–38.

[26] D. Losic, S. Simovic, Self-ordered nanopore and nanotube platforms for drug delivery applications, Expet Opin. Drug Deliv. 6 (2009) 1363–1381.

[27] A.I. Smirnov, O.G. Poluektov, Substrate-supported lipid nanotube arrays, J. Am. Chem. Soc. 125 (2003) 8434–8435.

[28] E.Y. Chekmenev, J. Hu, P.L. Gor'kov, W.W. Brey, T.A. Cross, A. Ruuge, A. I. Smirnov, 15N and 31P solid-state NMR study of transmembrane domain alignment of M2 protein of influenza A virus in hydrated cylindrical lipid bilayers confined to anodic aluminum oxide nanopores, J. Magn. Reson. 173 (2005) 322–327.

[29] A.M. Alaouie, A.I. Smirnov, Cooperativity and kinetics of phase transitions in nanopore-confined bilayers studied by differential scanning calorimetry, Biophys. J. 88 (2005) L11–L13.

[30] A.M. Alaouie, A.I. Smirnov, Formation of a ripple phase in nanotubular dimyristoylphosphatidylcholine Bilayers confined inside nanoporous aluminum oxide substrates observed by DSC, Langmuir 22 (2006) 5563–5565.

[31] E.Y. Chekmenev, P.L. Gor'kov, T.A. Cross, A.M. Alaouie, A.I. Smirnov, Flow-through lipid nanotube Arrays for structure-function studies of membrane proteins by solid-state NMR spectroscopy, Biophys. J. 91 (2006) 3076–3084.

[32] A. Marek, W. Tang, S. Milikisiyants, A.A. Nevzorov, A.I. Smirnov, Nanotube Array method for studying lipid-induced conformational changes of a membrane protein by solid-state NMR, Biophys. J. 108 (2015) 5–9.

[33] S. Milikisiyants, A.A. Nevzorov, A.I. Smirnov, Photonic band-gap resonators for high-field/high-frequency EPR of microliter-volume liquid aqueous samples, J. Magn. Reson. 296 (2018) 152–164.

[34] A.A. Nevzorov, A.I. Smirnov, Line narrowing in oriented-sample NMR of membrane proteins, in: L. Berliner (Ed.), Protein NMR: Modern Techniques and Biomedical Applications, 2015, pp. 159–185.

[35] H.-F. Chen, D.M. Gardner, R. Carmieli, M.R. Wasielewski, Controlling the orientation of spin-correlated radical pairs by covalent linkage to nanoporous anodic aluminum oxide membranes, Chem. Commun. 49 (2013) 8614–8616.

[36] T. Ming, S. Chang, Biomedical Applications of Immobilized Enzymes and Proteins, Plenum Press, New York, 1974, p. 448.

[37] J.S. McConnell, L.R. Hossner, pH-dependent adsorption isoterms of glyphosphate, J. Agric. Food Chem. 33 (1985) 1075–1078.

[38] A.G. Hemmersam, K. Rechendorff, F. Besenbacher, B. Kasemo, D.S. Sutherland, pH-dependent adsorption and conformational change of ferritin studied on metal oxide surfaces by a combination of QCM-D and AFM, J. Phys. Chem. C 112 (2008) 4180–4186.

[39] C. Helbing, R. Stoessel, D.A. Hering, M.M.L. Arras, J. Bossert, K.D. Jandt, pH-dependent ordered fibrinogen adsorption on polyethylene single crystals, Langmuir 32 (2016) 11868–11877.

[40] T.S. Varley, M. Hirani, G. Harrison, K.B. Holt, Nanodiamond surface redox chemistry: influence of physicochemical properties on catalytic processes, Faraday Discuss 172 (2014) 349–364.

[41] J.A. Rodríguez, M. Fernández-García, Synthesis, Properties, and Applications of Oxide Nanomaterials, JohnWiley & Sons, Inc., Hoboken, NJ, 2007, p. 752.

[42] G. Centi, R.A. van Santen, Catalysis for Renewables: from Feedstock to Energy Production, WILEY-VCH Verlag GmbH & Co. KGaA, Weinheim, 2007, p. 448.

[43] E.G. Kovaleva, L.S. Molochnikov, D.O. Antonov, D.P.T. Stepanova, M. Hartmann, A.N. Tsmokalyuk, A. Marek, A.I. Smirnov, Proton activity in nanochannels revealed by electron paramagnetic resonance of ionizable nitroxides: a test of the Poisson-Boltzmann double layer theory, J. Phys. Chem. C 122 (2018) 20527–20538.

[44] E.G. Kovaleva, L.S. Molochnikov, U. Venkatesan, A. Marek, D.P. Stepanova, K. V. Kozhikhova, M.A. Mironov, A.I. Smirnov, Acid-base properties of nanoconfined volumes of anodic aluminum oxide pores by EPR of pH-sensitive spin probes, J. Phys. Chem. C 120 (2016) 2703–2711.

[45] E.G. Kovaleva, L.S. Molochnikov, D.P. Stepanova, A.V. Pestov, D.G. Trofimov, I. A. Kirilyuk, A.I. Smirnov, Interfacial electrostatic properties of hydrated mesoporous and nanostructured alumina powders by spin labeling EPR, Cell Biochem. Biophys. 75 (2017) 159–170.

[46] T.I. Smirnova, M.A. Voinov, A.I. Smirnov, Spin probes and spin labels, in: Encyclopedia of Analytical Chemistry, John Wiley & Sons, Ltd, 2006.

[47] A.F. Gulla, D.E. Budil, Orientation dependence of electric field effects on the g-factor of nitroxides measured by 220 GHz EPR, J. Phys. Chem. B 105 (2001) 8056–8063.

[48] M.A. Voinov, I. Rivera-Rivera, A.I. Smirnov, Surface electrostatics of lipid bilayers by EPR of a pH-sensitive spin-labeled lipid, Biophys. J. 104 (2013) 106–116.

[49] V. Perelygin, M.A. Voinov, A. Marek, E.K. Ou, J. Krim, D. Brenner, T.I. Smirnova, A.I. Smirnov, Dielectric and electrostatic properties of the silica nanoparticle-water interface by EPR of pH-sensitive spin probes, J. Phys. Chem. C 123 (2019) 29972–29985.

[50] M.A. Voinov, A.I. Smirnov, Spin labels and spin probes for measurements of local pH and electrostatics by EPR, in: V. Chechik (Ed.), Electron Spin Resonance Specialist Periodical Reports, The Royal Society of Chemistry, Cambrige, UK, 2010, pp. 71–106.

[51] M.A. Voinov, A.I. Smirnov, Chapter seven - ionizable nitroxides for studying local electrostatic properties of lipid bilayers and protein systems by EPR, in: P.Z. Qin, K. Warncke (Eds.), Methods Enzymol., Academic Press, 2015, pp. 191–217.

[52] D.J. Stirland, R.W. Bicknell, Studies OF the structure OF anodic oxide films ON aluminum .1, J. Electrochem. Soc. 106 (1959) 481–485.

[53] M.K. McQuaig, A. Toro, W. Van Geertruyden, W.Z. Misiolek, The effect of high temperature heat treatment on the structure and properties of anodic aluminum oxide, J. Mater. Sci. 46 (2011) 243–253.

[54] J.W. Diggle, T.C. Downie, C.W. Goulding, Anodic oxide films on aluminum, Chem. Rev. 69 (1969) 365–405.

[55] Y. Xu, G.E. Thompson, G.C. Wood, B. Bethune, Anion incorporation and migration during barrier film formation on aluminium, Corrosion Sci. 27 (1987) 83–102.

[56] L. Fernández-Romero, J.M. Montero-Moreno, E. Pellicer, F. Peiró, A. Cornet, J. R. Morante, M. Sarret, C. Müller, Assessment of the thermal stability of anodic alumina membranes at high temperatures, Mater. Chem. Phys. 111 (2008) 542–547.

[57] A. Kirchner, K.J.D. MacKenzie, I.W.M. Brown, T. Kemmitt, M.E. Bowden, Structural characterisation of heat-treated anodic alumina membranes prepared using a simplified fabrication process, J. Membr. Sci. 287 (2007) 264–270.

[58] D. Wang, Y. Ruan, L. Zhang, W. Zhu, P. Wang, The thermal stability of anodic alumina membranes at high temperatures, Cryst. Res. Technol. 48 (2013) 348–354.

[59] A.I. Smirnov, R.L. Belford, Rapid quantitation from inhomogeneously broadened EPR spectra by a fast convolution algorithm, J. Magn. Reson., Ser. A 113 (1995) 65–73.

[60] T.I. Smirnova, A.I. Smirnov, R.B. Clarkson, R.L. Belford, Accuracy of oxygen measurements in T_2 (linewidth) EPR oximetry, Magn. Reson. Med. 33 (1995) 801–810.

[61] L.S. Molochnikov, E.G. Kovalyova, I.A. Grigor'ev, A.A. Zagorodni, Direct measurement of H^+ activity inside cross-linked functional polymers using nitroxide spin probes, J. Phys. Chem. B 108 (2004) 1302–1313.

[62] L.S. Molochnikov, E.G. Kovaleva, E.L. Golovkina, I.A. Kirilyuk, I.A. Grigor'ev, Spin probe study of acidity of inorganic materials, Colloid J. 69 (2007) 769–776.

[63] E.G. Kovaleva, L.S. Molochnikov, E.L. Golovkina, M. Hartmann, I.A. Kirilyuk, I. A. Grigor'ev, Dynamics of pH-sensitive nitroxide radicals in water adsorbed in ordered mesoporous molecular sieves by EPR spectroscopy, Microporous Mesoporous Mater. 179 (2013) 258–264.

[64] D.E. Budil, S. Lee, S. Saxena, J.H. Freed, Nonlinear-least-squares analysis of slow-motion EPR spectra in one and two dimensions using a modified Levenberg-Marquardt algorithm, J. Magn. Reson., Ser. A 120 (1996) 155–189.

[65] A.I. Smirnov, T.I. Smirnova, Resolving domains of interdigitated phospholipid membranes with 95 GHz spin labeling EPR, Appl. Magn. Reson. 21 (2001) 453–467.

[66] T.I. Smirnova, A.I. Smirnov, High-field ESR spectroscopy in membrane and protein biophysics, in: M.A. Hemminga, L.J. Berliner (Eds.), ESR Spectroscopy in Membrane Biophysics, Springer US, New York, 2007, pp. 165–251.

[67] R. Owenius, M. Engström, M. Lindgren, M. Huber, Influence of solvent polarity and hydrogen bonding on the EPR parameters of a nitroxide spin label studied by 9-GHz and 95-GHz EPR spectroscopy and DFT calculations, J. Phys. Chem. 105 (2001) 10967–10977.

[68] T.I. Smirnova, T.G. Chadwick, M.A. Voinov, O. Poluektov, J. van Tol, A. Ozarowski, G. Schaaf, M.M. Ryan, V.A. Bankaitis, Local polarity and hydrogen bonding inside the Sec14p phospholipid-binding cavity: high-field multi-frequency electron paramagnetic resonance studies, Biophys. J. 92 (2007) 3686–3695.

[69] E. Kovaleva, L. Molochnikov, V. Osipova, D. Stepanova, V. Reznikov, Electrosurface properties of nanostructured silica assessed by EPR of molecular pH labels, Appl. Magn. Reson. (2015) 1–16.

[70] E.A. Paukshtis, P.I. Soltanov, E.N. Yurchenko, K. Jiratova, Acid-base properties of modified aluminas, Collect. Czech Chem. Commun. 47 (1982) 2044–2060.

[71] C. Morterra, A. Chiorino, G. Ghiotti, E. Garrone, Surface-acidity of eta-alumina .1. Pyridine chemisorption at room-temperature, J. Chem. Soc. Faraday Trans. I 75 (1979) 271–288.

[72] H.K. Hall, Correlation of the base strengths of Amines1, J. Am. Chem. Soc. 79 (1957) 5441–5444.

[73] M.S. Fernandez, P. Fromherz, Lipoid pH indicators as probes of electrical potential and polarity in micelles, J. Phys. Chem. 81 (1977) 1755–1761.

[74] P. Fromherz, Lipid coumarin dye as a probe of interfacial electrical potential in biomembranes, Methods Enzymol. 171 (1989) 376–387.

[75] T.Y. Datsko, V.I. Zelentsov, Dependence of the surface charge and the fluorine adsorption by gamma-aluminum oxide on the solution temperature, Surf. Eng. Appl. Electrochem. 45 (2009) 404–410.

[76] R. Sprycha, Electrical double layer at alumina/electrolyte interface: I. Surface charge and zeta potential, J. Colloid Interface Sci. 127 (1989) 1–11.

[77] T.D. Pham, M. Kobayashi, Y. Adachi, Interfacial characterization of α-alumina with small surface area by streaming potential and chromatography, Colloids Surf. Physicochem. Eng. Aspects 436 (2013) 148–157.

[78] H. Leese, V. Bhurtun, K.P. Lee, D. Mattia, Wetting behaviour of hydrophilic and hydrophobic nanostructured porous anodic alumina, Colloid. Surface. Physicochem. Eng. Aspect. 420 (2013) 53–58.

[79] M.R. Das, J.M. Borah, W. Kunz, B.W. Ninham, S. Mahiuddin, Ion specificity of the zeta potential of α-alumina, and of the adsorption of p-hydroxybenzoate at the α-Alumina–water interface, J. Colloid Interface Sci. 344 (2010) 482–491.

[80] G.A. Parks, Isoelectric points of solid oxides, solid hydroxides and aqueous hydroxo complex systems, Chem. Rev. 65 (1965) 177–&.

[81] E. Yalamaç, A. Trapani, S. Akkurt, Sintering and microstructural investigation of gamma–alpha alumina powders, Engineering Science and Technology, Int. J. 17 (2014) 2–7.

[82] M.A. Voinov, C.T. Scheid, I.A. Kirilyuk, D.G. Trofimov, A.I. Smirnov, IKMTSL-PTE, a phospholipid-based EPR probe for surface electrostatic potential of biological interfaces at neutral pH: effects of temperature and effective dielectric constant of the solvent, J. Phys. Chem. B 121 (2017) 2443–2453.

[83] E. Kovaleva, L. Molochnikov, pH-sensitive nitroxide radicals for studying inorganic and organo-inorganic materials and systems, in: A.I. Kokorin (Ed.), Nitroxides - Theory, Experiment and Applications, InTech, Rijeka, Croatia, 2012, pp. 211–246.

[84] T.I. Smirnova, A.I. Smirnov, S.V. Paschenko, O.G. Poluektov, Geometry of hydrogen bonds formed by lipid bilayer nitroxide probes: a high-frequency pulsed ENDOR/EPR study, J. Am. Chem. Soc. 129 (2007) 3476–3477.

[85] E.G. Kovaleva, L.S. Molochnikov, E.L. Golovkina, M. Hartmann, I.A. Kirilyuk, I. A. Grigoriev, Electrical potential near hydrated surface of ordered mesoporous molecular sieves assessed by EPR of molecular pH-probes, Microporous Mesoporous Mater. 203 (2015) 1–7.

[86] B.J. Pedimonte, T. Moest, T. Luxbacher, C. von Wilmowsky, T. Fey, K.A. Schlegel, P. Greil, Morphological zeta-potential variation of nanoporous anodic alumina layers and cell adherence, Acta Biomater. 10 (2014) 968–974.

[87] J.J. Fitzgerald, G. Piedra, S.F. Dec, M. Seger, G.E. Maciel, Dehydration studies of a high-surface-area alumina (Pseudo-boehmite) using solid-state 1H and 27Al NMR, J. Am. Chem. Soc. 119 (1997) 7832–7842.

[88] K. Wefers, C. Misra, Oxides and hydroxides of aluminum, in: Alcoa Laboratories, 1987, pp. 1–92.

[89] Z. Zhang, R.W. Hicks, T.R. Pauly, T.J. Pinnavaia, Mesostructured forms of γ-Al2O3, J. Am. Chem. Soc. 124 (2002) 1592–1593.

[90] J.W. Ntalikwa, Determination of surface charge density of alpha-alumina by acid-base titration, Bull. Chem. Soc. Ethiop. 21 (2007) 117–128.

[91] F. Le Coz, L. Arurault, S. Fontorbes, V. Vilar, L. Datas, P. Winterton, Chemical composition and structural changes of porous templates obtained by anodising aluminium in phosphoric acid electrolyte, Surf. Interface Anal. 42 (2010) 227–233.

[92] I. Levin, D. Brandon, Metastable alumina polymorphs: crystal structures and transition sequences, J. Am. Ceram. Soc. 81 (1998) 1995–2012.

[93] M. Robinson, J.A. Pask, D.W. Fuerstenau, Surface charge of alumina and magnesia in aqueous media, J. Am. Ceram. Soc. 47 (1964) 516–520.